ADVANCED QUANTUM TECHNOLOGIES
www.advquantumtech.com

Decoherence of Single-Excitation Entanglement over Duan-Lukin-Cirac-Zoller Quantum Networks Caused by Slow-Magnetic-Field Fluctuations and Protection Approach

Can Sun, Ya Li, Yi-bo Hou, Min-jie Wang, Shu-jing Li, and Hai Wang**

Atomic spin-wave (SW) memory is a building block for quantum repeater. However, due to decoherence caused by atomic motions and magnetic-field gradients, SW retrieval efficiency decays with storage time. Slow magnetic-field fluctuations (SMFFs) lead to shot-to-shot phase noises of SWs, but have not been considered in previous repeater protocols. Here, a SW model including a homogeneous phase noise caused by SMFFs is developed, and then revealed that such phase noise induces decoherence of single-excitation entanglement between two atomic ensembles in a repeater link. For verifying this conclusion, single-excitation entanglement between two SWs in a cold atomic ensemble is experimentally prepared and observed entanglement decoherence induced by SMFFs. Limited by SMFFs, the evaluated lifetime of the single-excitation entanglement over a repeater link is ≈135 ms, even if the link uses optical-lattice atoms as nodes. Then an approach that may overcome such limitations and extend this lifetime to ≈1.7 s is presented.

1. Introduction

Quantum repeaters (QRs) hold promise for realizing long-distance quantum communication,[1,2] large-scale quantum networks (QNs),[3–6] and longer-baseline telescopes [7]. In the QR protocol,[8] a long distance, over which entanglement is required to be distributed, is divided into N shorter elementary links. Entanglement is at first created between two quantum memories (nodes) in elementary links and then extended over full distance via entanglement swapping. In the past two decades, various physical systems[9] such as atomic ensembles[2,10] and single quantum systems, including single atoms,[11,12] ions[13–15] and solid-state spins[16–18] have been developed as memory nodes. The atomic-ensemble-based quantum memories (QMs) can be efficiently mapped into photons[1–3,19] and then hold promise for entanglement swapping. The well-known Duan-Lukin-Cirac-Zoller (DLCZ) protocol is a QR architecture based on atomic ensembles.[1,2] It creates spin-wave (SW) memory via spontaneous Raman emission, which simultaneously emits a Stoke photon correlated with the SW memory. Significant progress has been achieved on experimental generations of non-classically correlated or entangled pairs of a photon and a SW via DLCZ protocol.[20–42] Alternately, the non-classically correlated or entangled pairs can be achieved by using the SPDC process together with quantum memories,[43–47] where, the quantum memories are realized via "absorptive" ("read-write"[48]) storage schemes that are based on electromagnetically induced transparency,[43] atomic frequency comb (AFC)[44–46] and off-resonant cascaded absorption[47] et al. AFC quantum memories are demonstrated with rare-earth ions doped (REID) crystals, which have large bandwidth and are available for temporally- and spectrally- multiplexed storages.[6] In the past two decades, significant progresses on AFC memories storing multiplexed temporal and/or spectral modes have been experimentally made.[32,33,46,49] DLCZ memories promise spatially-multiplexed storages, which have also been experimentally demonstrated in the past years.[39–42]

With the atom-photon quantum interfaces, entanglement between two memories (nodes), which forms an elementary repeater link, have been demonstrated. Based on the detection at a central station of a single Stokes photon that comes from one of two remote ensembles,[50,51] entanglement between the two atomic ensembles has been generated via single photon Bell measurement. Such entanglement generation relies on single-photon interferometers (SPI). Thus, it requires stabilizing the phase difference between two arms of the interferometers.[2] Entanglement between two memories can also be established by a two-photon-interference (TPI) scheme,[52–55] which uses

C. Sun, Y. Li, Y.-bo Hou, M.-jie Wang, S.-jing Li, H. Wang
State Key Laboratory of Quantum Optics and Quantum Optics Devices, Institute of Opto-Electronics
Taiyuan 030006, China
E-mail: lishujing@sxu.edu.cn; wanghai@sxu.edu.cn
C. Sun, Y. Li, Y.-bo Hou, M.-jie Wang, S.-jing Li, H. Wang
Collaborative Innovation Center of Extreme Optics
Shanxi University
Taiyuan 030006, China

The ORCID identification number(s) for the author(s) of this article can be found under https://doi.org/10.1002/qute.202300148

© 2023 The Authors. Advanced Quantum Technologies published by Wiley-VCH GmbH. This is an open access article under the terms of the Creative Commons Attribution-NonCommercial-NoDerivs License, which permits use and distribution in any medium, provided the original work is properly cited, the use is non-commercial and no modifications or adaptations are made.

DOI: 10.1002/qute.202300148

atom-photon entanglement in each node and removes the requirement for the long-distance phase stability in SPI schemes.[55] However, TPI scheme requires detecting two photons, which leads to a much lower probability of elementary entanglement generation compared to that via SPI.[52]

Entanglement between two remote memories in a link has been demonstrated with atomic ensembles[50–54,56–59] or single quantum systems including individual atoms,[60,61] ions,[15] and solid-state spins.[16–18] Also, by distributing entangled pairs of two photons[62] or of a SW and a photon over two nodes as links,[63] entanglement connections between repeater links have been experimentally demonstrated. So far, QRs still face the challenges including the deterministic entanglement generation between two atomic memories with a separation long distance (for example 100 km) and the connection of two or more repeater links formed by matter nodes. To overcome such challenges, it is required to store entanglement for a long time and effectively retrieve the photons stored in memories.[3]

To achieve long-lived QMs based on atomic ensembles, decoherence mechanisms of SWs in cold atomic ensembles have been studied, and two main decoherence processes have been revealed.[22–24] One process is due to atomic motions, which make atoms move out of spin-wave spatial mode in the atomic ensembles or lead to the dephasing of spin wave.[24] Another process results from gradients of magnetic fields,[22,23] which make spin transitions of the atoms at different positions experience inhomogeneous broadening and then lead to a loss of quantum phase in collective superpositions. Atomic-motion-induced decoherence can be suppressed either by lengthening spin-wave wavelengths[24,39,41,64] or confining the atoms in optical lattices.[26,27,36,38,63] Inhomogeneous-broadening-induced decoherence can be suppressed by storing SWs in magnetic-field-insensitive (or "clock") spin transitions.[23,27,36,38,39,41] Based on these schemes of suppressing decoherence, the storage times at $1/e$ retrieval efficiency for spin-wave QMs reach to ≈400 ms in optical-lattice atoms.[38] It has been experimentally demonstrated that fidelities of entanglement between two ensembles[25] and polarization atom-photon entanglement[35] decay with time, respectively, due to the decoherence processes.

Decoherence mechanisms of memories in REID crystals have been also studied in recent years. Contrary to the coherence stored in the gas-state ensemble, the coherence stored in REID crystals do not suffer from atomic diffusion.[65] There are two main decoherence process in the storages of REID crystals,[65–67] one comes from the inhomogeneous broadening of the spin transition due to gradient magnetic fields, and another is the variations of the spin transition frequency over time, due to magnetic field fluctuations of the ion's environment. By means of a zero-first-order-Zeeman (ZEFOZ) magnetic-field scheme and using dynamical decoupling (DD) to suppress decoherence, the lifetimes of AFC storages of weak coherent light pulses reach 1min in Pr^{3+} :Y_2SiO_5[65] and 1 h in $^{151}Eu^{3+}$:Y_2SiO_5 crystals,[68] respectively. The longest coherence time of AFC memory for a single-photon level pulse in a $^{151}Eu^{3+}$:Y_2SiO_5 crystal reaches ≈20 ms.[69]

On the other hand, slow magnetic-field fluctuations (SMFFs) will induce shot-to-shot phase fluctuations of atomic memory. In quantum systems such as trapped single atoms and NV centers, the phase noise of the atomic memory qubit caused by SMFFs has been pointed out,[11,12,17] and dynamical decoupling strategies have been developed to suppress such phase noise.[12,17] Quantum storages of weak coherence light with arbitrary polarization based on EIT scheme in an ultra-cold atomic ensemble (BEC) have been demonstrated and the polarization fidelity decay caused by SMFFs has been reported.[70] By compensating the magnetic-field fluctuations with an open-loop feed-forward circuit, the long-lived optical polarization storage was achieved in that experiment. In a recent experiment on entanglement generation between two atomic ensembles,[59] decoherence of a SW memory for polarization qubit caused by SMFFs is observed, where, SMFFs are mainly produced by ac noise of Helmholtz coils. By synchronizing the experimental sequence with the main electricity frequency 50 Hz, the qubit decoherence was significantly suppressed in that experiment.[59] However, so far, the SW phase noise caused by SMFFs has not been modeled and its influence on entanglement between two atomic ensembles in DLCZ-like links has not been demonstrated.

In the presented work, we develop a SW model that includes phase noise induced by SMFFs. Such phase noise is homogeneous for each SW superposition and then will not affect SW retrieval efficiency at any storage time. While, SMFFs will lead to the phase-noise difference between two ensembles in a repeater link and then degrade the single-excitation entanglement between the ensembles. For verifying this conclusion, we experimentally generate two single-excitation entanglement states between SWs in a cold atomic ensemble. By measuring the visibility of interference between entangled two SWs, where, two SWs are stored in a magnetic-field-sensitive and a "clock" spin transition, respectively, we observe that coherence between the SWs decays with storage time. We also demonstrate that the phase-noise difference between entangled two SWs is eliminated when both SWs are stored in the same magnetic-field-sensitive transitions. Based on our SW model and previous experimental data in refs.[38, 71], we predict that the lifetime of single-excitation entanglement between two ensembles is mainly limited to decoherence induced by SMFFs. Even if the link uses optical-lattice atoms as memory nodes, the lifetime of entanglement over a repeater link is limited by ≈135 ms. We finally propose a scheme that can cancel the phase-noise difference, where a single DC supply is used to drive the Helmholtz coils of two nodes and then make the magnetic fields fluctuation at both nodes be the same.

2. Theoretical Analysis: Decoherence of Single-Excitation Entanglement Between Two Atomic Ensembles Caused by SMFFs

At first, we develop a SW model that includes amplitude and phase decoherence. As shown in **Figure 1**, the generation of SW is based on DLCZ process. A write laser pulse is applied to an ensemble of N atoms with three-level structure, which creates a non-classically correlated pairs of a Stokes photon and a spin wave. When excitation probability $\chi << 1$, the atom-photon system is written as[2,25]

$$\Phi_{a,p} = |0\rangle + \sqrt{\chi}|1\rangle_p |\psi_a(0)\rangle + O(\chi) \quad (1)$$

where, $|0\rangle$ denotes the vacuum part, $|1\rangle_p$ one photon in the Stokes field, $|\psi_a(0)\rangle$represents a SW formed by a coherent superposition

© 2023 The Authors. Advanced Quantum Technologies published by Wiley-VCH GmbH

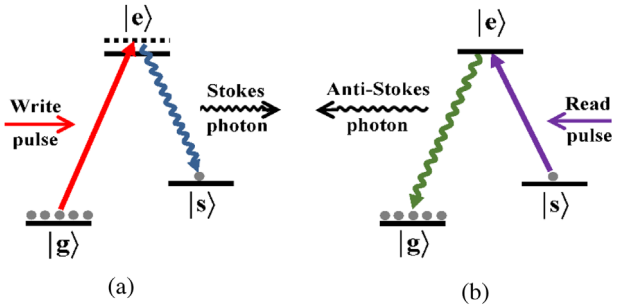

Figure 1. Atomic levels related to the write a) and read b) processes in the DLCZ scheme, respectively.

of all the possible states with N-1 atoms in $|g\rangle$ and one atom in $|s\rangle$ and is written as,

$$|\psi_a(0)\rangle = \frac{1}{\sqrt{N}} \sum_{j=1}^{N} e^{-i\Delta k z_j(0)} |g\rangle_1 |g\rangle_2 \ldots |s\rangle_j \ldots |g\rangle_N \tag{2}$$

where, $z_j(0)$ is the j-th atom coordinate at storage time $t = 0$, $\Delta k = (k_w - k_s)$ the SW wave-vector, k_w is the wave-vector of the write beam, whose frequency is slightly detuned from the $|g\rangle \rightarrow |e\rangle$ transition, k_S the wave-vector of the Stokes photon, which is emitted on the $|g\rangle \rightarrow |e\rangle$ transition. The magnetic field in the atoms is generated by applying a DC supply to Helmholtz coils. It is along z direction and can be written as $\vec{B} = (B_0 + B'z + \delta B(t,z))\vec{z}$, where, B_0 is the bias magnetic field, $B'$is the gradient of the magnetic field, $\delta B(t,z)$ represents slow magnetic-field fluctuations (SMFFs). After storage time t, the spin wave is evolved into

$$|\psi_a(t)\rangle = \frac{1}{\sqrt{N}} e^{-i\omega_0 t} \sum_{j=1}^{N} e^{-i\Delta\omega(z_j)t - i\Delta k\left[z_{j(0)} + \delta z_j(t)\right] - i\delta\varphi(z_j,t)} \times |g\rangle_1 |g\rangle_2 \ldots |s\rangle_j \ldots |g\rangle_N \tag{3}$$

where, ω_0 is the Larmor frequency of the used spin transition $|g, m_{Fg}\rangle \leftrightarrow |s, m_{Fs}\rangle$caused by the bias field$B_0$, $\Delta\omega(z_j) = 2\pi\mu' B' z_j$ denotes Larmor frequency shifts of the atoms at the position z_j, which results in the inhomogeneous broadening of the spin transition, $\mu' = dv/dB$ corresponds to the sensitivity of the spin transition $|g, m_{Fg}\rangle \leftrightarrow |s, m_{Fs}\rangle$to the magnetic field, v is the frequency of the spin transition, and $\delta\varphi(z_j,t) = 2\pi \int_0^t \mu' \delta B(z_j,t')dt'$ denotes the phase noise of the atom induced by SMFF $\delta B(z_j,t)$ at the position z_j. $\delta B(z_j,t)$ mainly results from the current fluctuation of the DC supply and also includes a small ac noise of environment field. The frequencies of the coils range from 200 Hz to 0 Hz,[72] and the wavelength of the magnetic-field fluctuations $\delta B(t,z)$ is more than $1500km$, which far exceeds the length (≈5 mm) of the ensemble. So, SMFF remains the same value for all of the atoms, i.e., $\delta B(z_j,t) = \delta B(t)$ and $\delta\varphi(z_j,t) = \delta\varphi(t) = 2\pi \int_0^t \mu' \delta B(t')dt'$. Thus, the SW is rewritten as

$$|\psi_a(t)\rangle = \frac{1}{\sqrt{N}} e^{-i\omega_0 t - i\delta\varphi(t)} \sum_{j=1}^{N} e^{-i\Delta\omega(z_j)t - i\Delta k\left[z_{j(0)} + \delta z_j(t)\right]} \times |g\rangle_1 |g\rangle_2 \ldots |s\rangle_j \ldots |g\rangle_N \tag{4}$$

As pointed out in ref.[70], the main contributions of the phase noise $\delta\varphi(t)$ can be assumed to result from shot-to-shot fluctuations $\delta B(t)$, i.e., for an individual trial with a storage time t, $\delta\varphi(t) = 2\pi\mu'\delta B t$. We assume that the magnetic-field fluctuations δB follow Lorentzian distribution:

$$P(\delta B) = \frac{\sigma_B/\pi}{\delta B^2 + \sigma_B^2} \tag{5}$$

where, σ_B is the rms width of the Lorentzian distribution. The spin wave at storage time t can be rewritten as:

$$|\psi_a(t)\rangle = |\psi_a(0)\rangle \langle\psi_a(0)|\psi_a(t)\rangle = e^{-i\omega_0 t - i\delta\varphi(t)} D(t) |\psi_a(0)\rangle, \tag{6}$$

where, $D(t) = \sum_{j=1}^{N} e^{-i\Delta\omega(z_j)t - i\Delta k v_j t} = e^{-t^2/2\tau_1^2} e^{-t^2/2\tau_2^2} = e^{-t^2/2\tau_D^2}$, which denotes SW amplitude factor, where, τ_1 and τ_2 are the lifetimes limited by decoherence arising from atomic random motions (see ref.[24] or Supporting information) and the inhomogeneous broadening of the spin transition caused by the gradient B' (see ref.[23] or Supporting information), respectively, $\tau_D = (\frac{\tau_1\tau_2}{\sqrt{\tau_1^2+\tau_2^2}})$ is the total lifetime. The SW can be retrieved by a read pulse with the retrieval efficiency[24]

$$\gamma(t) = \gamma_0 \left|\langle\psi_a(0)|\psi_a(t)\rangle\right|^2 = \gamma_0 |D(t)|^2 = \gamma_0 e^{-t^2/\tau_D^2} \tag{7}$$

where, $\gamma_0 \leq 1$ denotes the zero-delay retrieval efficiency. The Equation (6) shows that SMFFs have not led to decay of SW retrieval efficiency. However, we identify that it will induce decoherence of the single-excitation entangled state between two or multiple SW memories.

Figure 2 shows the sketch of generating single-excitation entanglement between two remote atomic ensembles via DLCZ protocol. Two ensembles R and L, which use the same-species atoms, are simultaneously applied by write pulses w_R and w_L, respectively. The emitted Stokes fields a_{S_R} and a_{S_L} from the ensembles R and L are sent to a center station and combined at a 50/50 beam splitter (labeled as BS_S). The output fields of BS_S are written as $a_{S1} = (a_{S_R} + a_{S_L})/\sqrt{2}$ and $a_{S2} = (a_{S_R} - a_{S_L})/\sqrt{2}$, which are directed into detectors D_{S1} and D_{S2}, respectively. In the ideal case, a successful detection at detectors D_{S1} or D_{S2} after BS_S projects the two ensembles into an entangled state[50]:

$$\Psi_{R,L}(0) = \left(e^{-i\eta_w} |1\rangle_R |0\rangle_L \pm |0\rangle_R |1\rangle_L\right)/\sqrt{2} \tag{8}$$

where, $|1\rangle_{R(L)} = \psi_{R(L)}(t=0)$ refers to the SW state in the ensemble R (L), which corresponds to an excitation, $|0\rangle_{R(L)} = \otimes_j |g_j\rangle_{R(L)}$ denotes the ground state of the ensemble R (L), $\eta_w = \Delta\phi_w + \Delta\beta_S$, $\Delta\phi_w$ is the phase difference between the write beams from a beam splitter (BS_w, which is not marked in Figure 2) to the ensembles R and L, and $\Delta\beta_S$ the phase difference between Stokes (write-out) fields a_{S_R} and a_{S_L} in propagation from the ensembles to the beam splitter BS_S. After a storage time t, the heralded entanglement state is evolved to

$$\Psi_{R,L}(t) = e^{-i\omega_0 t} e^{-i\delta\varphi_R(t)} D(t) \left(e^{-i\eta_w} |1\rangle_R |0\rangle_L \pm e^{i[\delta\varphi_R(t) - \delta\varphi_L(t)]} |0\rangle_R |1\rangle_L\right)/\sqrt{2} \tag{9}$$

© 2023 The Authors. Advanced Quantum Technologies published by Wiley-VCH GmbH

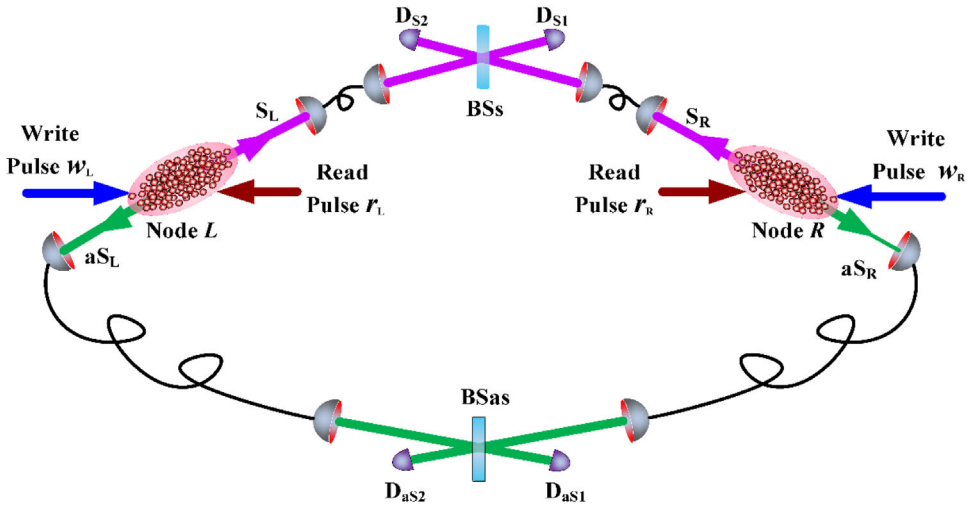

Figure 2. Single-excitation entanglement generation between two atomic ensembles R and L in a repeater link. A write (read) laser pulse is split into write (read) pulses $w_L(r_L)$ and $w_R(r_R)$ by a beam splitter BS_w (BS_r). For simplicity, we didn't mark BS_w (BS_r) in the figure. The write and read pulses w_R and r_R (w_L and r_L) counter propagate and are applied to the ensembles R (L). The write pulse w_R (w_L) creates the Stokes field a_{S_R} (a_{S_L}) and SW $|1_R\rangle$ ($|1_L\rangle$) respectively. The Stokes field a_{S_R} and a_{S_L} are sent to a 50/50 beam splitter (BS_S). The SWs $|1_R\rangle$ and $|1_L\rangle$ are retrieved by read pulses r_R and r_L, respectively. The retrieved fields a_{aS_R} and a_{aS_L} are sent to another 50/50 beam splitter (BS_{aS}). The beam splitters BS_S and BS_{aS} (BS_W and BS_R) form Stokes-anti-Stokes field (write-read laser) interferometer. The difference of two arms of each interferometer is actively stabilized. Single-photon detectors D_{S1} and D_{S2} (D_{aS1} and D_{aS2}) are used to detect the Stokes (anti-Stokes) fields.

where, we assume that Larmor frequencies caused by the bias magnetic field in R and L ensembles have the same value ω_0, the decay factors for $|1\rangle_R$ and $|1\rangle_L$ are assumed to be $D_R(t) = D_L(t) = D(t)$, the retrieval efficiencies $\gamma_R(t) = \gamma_L(t) = \gamma_0|D(t)|^2 = \gamma(t)$, the phase noise $\delta\varphi_R(t) = 2\pi\mu'\delta B_R t$ and $\delta\varphi_L(t) = 2\pi\mu'\delta B_L t$, $\delta B_R(t)$ and $\delta B_L(t)$ are SMFFs in the ensembles R and L, respectively, whose Lorentzian distribution are assumed to have the same rms width $\sigma_R = \sigma_L = \sigma_B$. The entanglement state may be verified following the protocol in Refs,[25,49] where, read beams are applied into the two ensembles to convert the spin waves $\psi_R(t)$and $\psi_L(t)$ into anti-Stokes fields a_{aS_R} and a_{aS_L}, respectively. In the ideal case, the atomic state $\Psi_{R,L}(t)$ is directly converted to the photonic entangled state $\Phi_{R,L}$. The entanglement degree of $\Psi_{R,L}(t)$ or $\Phi_{R,L}$ can be characterized by the concurrence[25,49]

$$C = \max\left(0, \frac{2d - 2\sqrt{p_{00}p_{11}}}{P}\right) \tag{10}$$

where, p_{ij} corresponds to the probability to find i photons in the field $a_{aS_L}$and j photons in the field a_{aS_R},$P = p_{01} + p_{10} + p_{00} + p_{11}$, $d = V(p_{01} + p_{10})/2$ is the coherence term between the states $|1\rangle_R|0\rangle_L$ and $|0\rangle_R|1\rangle_L$, V is the visibility of the interference fringes between the anti-Stokes fields a_{aS_L} and a_{aS_R} when the relative phase θ between the fields is scanned. The concurrence C ranges from 0 for a separable state to 1 for a maximally entangled state.[25] The probabilities of p_{ij} can be directly measured via photon counting in the fields a_{aS_L} and a_{aS_R}. The measurement of V requires to combine the two retrieved fields on a 50/50 beam splitter, which is labeled as BS_{aS} in Figure 2. After BS_{aS}, the output modes $a_{aS1} = (a_{aS_R} + a_{aS_L})/\sqrt{2}anda_{aS2} = (a_{aS_R} - a_{aS_L})/\sqrt{2}$ are directed to single-photon detectors D_{aS1} and D_{aS2}, respectively. The visibility V can be measured as[73]

$$V = \frac{\mathrm{Max}\left\{P_{S1,aS1}(\theta)\right\} - Min\left\{P_{S1,aS1}(\theta)\right\}}{\mathrm{Max}\left\{P_{S1,aS1}(\theta)\right\} + Min\left\{P_{S1,aS1}(\theta)\right\}} \tag{11}$$

where, $\mathrm{Max}\{P_{S1,aS1}(\theta)\}$ ($Min\{P_{S1,aS1}(\theta)\}$) denotes the maximum (minimum) coincidence detection between the Stokes and anti-Stokes fields a_{S1} and a_{aS1} when scanning θ. The probability $P_{S1,aS1}(\theta)$ is found to be (see Equation (S9), Supporting information)

$$P_{S1,aS1}(\theta) = \chi\gamma(t)\eta^2\left(1 + e^{-t/\tau_0}\cos\theta\right)/2 + P_S P_{aS} \tag{12}$$

where, χ ($\gamma(t)$) is excitation probability (retrieval efficiency) for either ensemble alone, with $\chi_R = \chi_L = \chi$ ($\gamma_R = \gamma_L = \gamma$) assumed, η denotes the detection efficiency of the detectors (D_{S1}, D_{aS2}, D_{S1} and D_{aS2}), $\tau_0 = [2\pi\mu'\sigma_\Delta]^{-1}$ is the lifetime of the coherence between the two SWs, $\sigma_\Delta = 2\sigma_B$ is the relative width of SMFFs between the two ensembles, and $P_S(P_{aS})$ the probability of detecting a photon in the Stokes field a_S (anti-Stokes field a_{aS}) for either ensemble, with $P_{S_L} = P_{S_R} = P_S$ ($P_{aS_L} = P_{aS_R} = P_{aS}$) assumed. The visibility is then found to be [see Supporting Information for details]

$$V = \frac{g_{S,aS} - 1}{g_{S,aS} + 1}e^{-t/\tau_0} \tag{13}$$

where, the factor e^{-t/τ_0} describes exponential decay of the entanglement state with t due to SMFFs, $g_{S,aS}$ denotes the cross-correlation function between Stokes and anti-Stokes fields for either ensemble alone (see Equation (S11) in Supporting information). In the previous work of ref. [25], the visibility of the

© 2023 The Authors. Advanced Quantum Technologies published by Wiley-VCH GmbH

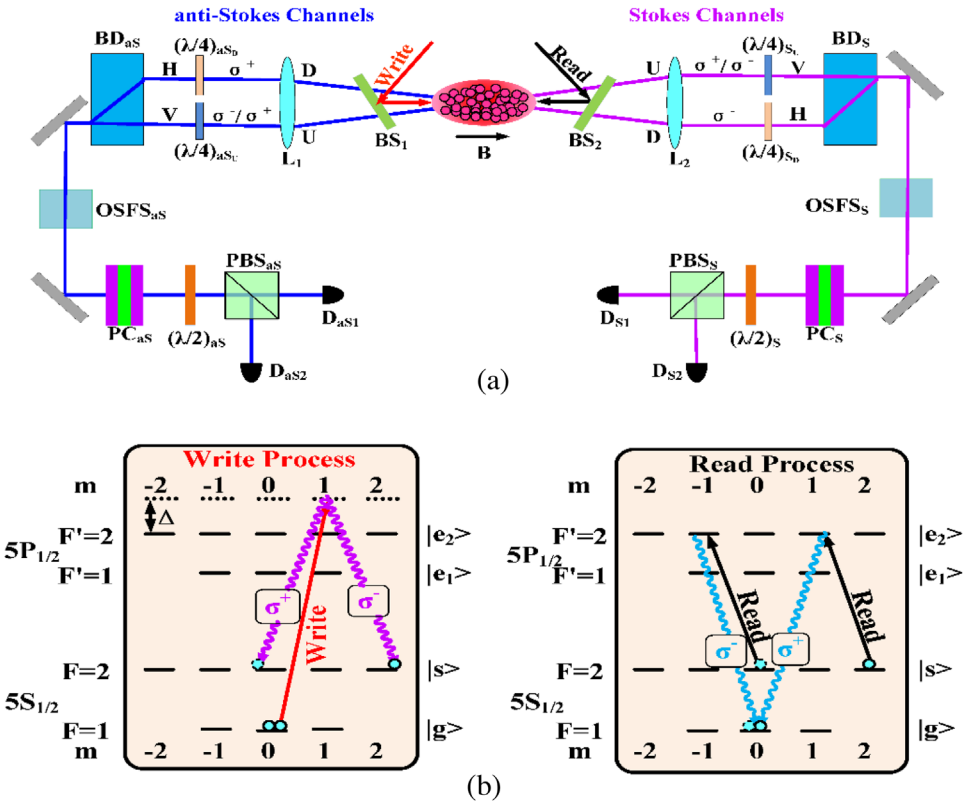

Figure 3. a) Experimental setups for generating entanglement states. BD_S (BD_{aS}): beam displacer; BS_1 (BS_2): non-polarizer beam splitter; L_1 (L_2): lens; $OSFS_S$ ($OSFS_{aS}$): optical spectrum filter systems for Stokes (anti-Stokes) channel; PC_S (PC_{aS}): phase compensator[39]; $(\lambda/4)_{S_{U(D)}}$ and $(\lambda/4)_{aS_{U(D)}}$: quarter-wave plates; $(\lambda/2)_{S(aS)}$: half-wave plate. BD_S and BD_{aS} form the Stokes-anti-Stokes interferometer. U and D denote the two arms of the interferometer. A σ^+-polarized write pulse is applied to the MOT atoms through BS_1, which induces spontaneous Raman scattering of $\sigma^+$and/or σ^--polarized Stokes photons and create simultaneously SWs. For the generation of the first (second) entanglement state, the $\sigma^+(\sigma^-)$-polarized photon propagating along U arm is changed into *V*-polarization after $(\lambda/4)_{S_U}$. In the D arm, the σ^--polarized photon is changed into *H*-polarization after $(\lambda/4)_{S_D}$. The *V*-polarized photon in U arm and *H*-polarized photon in D arm are combined by BD_S. b) Relevant levels for write and read processes.

single-excitation entangle state is described as $V = \frac{g_{S,aS}-1}{g_{S,aS}+1}$, which doesn't involve the dephasing induced by SMFFs. Contrast to that work, our Equation (13) shows that the visibility of single-excitation entanglement between two ensembles suffers from not only the decoherence due to atomic motions and the inhomogeneous broadening, but also shot-to-shot phase noise caused by SMFFs.

In the following, we demonstrate a proof-in-principle experiment to verify the inference of Equation (13).

3. Experimentally Demonstrating Decoherence of Single-Excitation Entanglement Between Two SW Memories Caused by SMFFs in a Cold Atomic Ensemble

The experimental setup is illustrated in **Figure 3**a, which mainly includes a polarization interferometer and a cloud of cold ^{87}Rb atoms trapped in a magneto-optical trap (MOT). The interferometer is formed by two beam displacers (BD_{aS} and BD_S) with the cold atomic ensemble centered between them. The relevant levels of the atoms are shown in Figure 3b, where $|g\rangle = |5S_{1/2}, F = 1\rangle$, $|s\rangle = |5S_{1/2}, F = 2\rangle$, $|e_1\rangle = |5P_{1/2}, F' = 1\rangle$, and $|e_2\rangle = |5P_{1/2}, F' = 2\rangle$. The experiment is carried out in a cycle fashion. In each cycle, the magneto-optical trap (MOT) is switched on for 23 ms for preparing the cold atoms and then switched off for 10 ms for single-excitation entanglement generation. Before the entanglement generation, we apply a bias magnetic field ($B_0 \approx 1G$) onto the atoms along *z*-axis by using Helmholtz coils (with a size of $\sim 300mm$), which is driven by a DC power supply. At the same time, we apply pump laser pulses to prepare the atoms into initial Zeeman state $|g, m_F = 0\rangle$. The magnetic field along z-axis has a slow fluctuation of $\delta B$with a rms width of σ_B. We then start entanglement-generation trials. In the beginning of each trial, we apply a σ^+-polarized write pulse with frequency +140 MHz detuned from $|a\rangle \rightarrow |e_2\rangle$ transition through a beam splitter BS_1 (see Figure 3a). The write pulse induces the Raman transition $|g, m_F = 0\rangle \rightarrow |s, m_F = 0\rangle$ ($|g, m_F = 0\rangle \rightarrow |s, m_F = +2\rangle$) via $|e_2, m_F = +1\rangle$, which emits $\sigma^+(\sigma^-)$ -polarized Stokes photons and simultaneously creates SWs associated with the magnetic-field-insensitive (magnetic-field-sensitive) coherence between $|g, m_F = 0\rangle \leftrightarrow |s, m_F = 0\rangle$ ($|g, m_F = 0\rangle \leftrightarrow |s, m_F = +2\rangle$). If a Stokes photon is emitted into the arm *U* (*D*) of the

© 2023 The Authors. Advanced Quantum Technologies published by Wiley-VCH GmbH

interferometer, a collective (SW) excitation will be created in the mode M_U (M_D) with the wave-vector defined by $k_{M_U} = k_w - k_{S_U}$ ($k_{M_D} = k_w - k_{S_D}$), where, k_w denotes the wave-vector of write beam, k_{S_U} (k_{S_D}) denotes the wave-vector of the Stokes photon S_U (S_D) emitting into the arm U (D). For suppressing atom-motion-induced decoherence,[39] we set the angles between the wave-vectors k_w and $k_{S_{U(D)}}$ to be small values of $\pm 0.7^0$.

We generate two kinds of heralded entanglement states between two SWs. The first entangled state stores the two SWs in magnetic-field-insensitive (MFI) and magnetic-field-sensitive (MFS) spin transitions, respectively. We use this state to demonstrate entanglement degradation induced by SMFFs. In this entanglement generation, the σ^+-polarized (σ^--polarized) Stokes photons S_U (S_D) go through a wave plate $(\lambda/4)_{S_U}$ ($(\lambda/4)_{S_D}$). By setting the polarization angles of $(\lambda/4)_{S_U}$ and $(\lambda/4)_{S_D}$, we change the $\sigma^+$and σ^--polarized S_U and S_D into V and H–polarization, respectively. The V–polarized S_U and H–polarized S_D fields are combined into a spatial mode S by BD_S. The field S goes through a wave plate $(\lambda/2)_S$ and a polarization beam splitter PBS_S (see Figure 3a). With $(\lambda/2)_S$ at $\vartheta = 22.5^0$, PBS_S splits the input S field into two modes $a_{S1} = (a_{S_U} + a_{S_D})/\sqrt{2}$ and $a_{S2} = (a_{S_U} - a_{S_D})/\sqrt{2}$, which are directed to detectors D_{S1} and D_{S2}, respectively. Upon a detection event at D_{S1} in the ideal case with excitation probability $\chi = \chi_{M_U} \approx \chi_{M_D} \leq 1$, the two SWs are created in M_U and M_D modes and projected into the entangled state:

$$\Psi^{\uparrow,\downarrow}_{M_{U,D}}(0) = \left(e^{-i\Delta\phi_s}\,|1\rangle^{\uparrow}_{M_U}|0\rangle + |0\rangle\,|1\rangle^{\downarrow}_{M_D}\right)/\sqrt{2} + O(\chi) \tag{14}$$

where, labels $\uparrow$ and $\downarrow$ denote the SWs associated with the MFI and MFS, respectively, $|1\rangle$ denotes one collective excitation, $\Delta\phi_S$is the phase difference between two Stokes fields in propagation from the ensemble to BD_S. After a storage time t, the heralded entanglement state is evolved to:

$$\Psi^{\uparrow,\downarrow}_{M_{U,D}}(t) = D_0(t)e^{-i\omega_{U0}t - i\delta\varphi_U(t)}\left(e^{-i\Delta\phi_s}|1\rangle^{\uparrow}_{M_U}|0\rangle + e^{-i\Delta\omega_0 t - i\left[\delta\varphi_D(t) - \delta\varphi_U(t)\right]}|0\rangle|1\rangle^{\downarrow}_{M_D}\right)/\sqrt{2} \tag{15}$$

where, $\Delta\omega_0 = \omega_{D0} - \omega_{U0}$ denotes the frequency difference of Larmor precessions of SWs between M_U and M_D modes under the bias field B_0, $\delta\varphi_{U(D)}(t) = 2\pi\mu'_{U(D)}\delta B t$ denotes the phase noise of the SW in M_U (M_D) mode caused by δB. The sensitivities of the MFI spin wave $|1\rangle^{\uparrow}_{M_U}$ and MFS spin wave $|1\rangle^{\downarrow}_{M_D}$ can be evaluated as $\mu'_U \approx 0$ and $\mu'_D = \frac{\mu_B}{h}$ respectively. Finally, we have $\delta\varphi_D(t) - \delta\varphi_U(t) = \delta\varphi(t) \approx 2\pi\frac{\mu_B}{h}\delta B t$ and $\Delta\omega_0 = \frac{2\pi\mu_B}{h}B_0$. For simplicity, we have assumed that the amplitude-decay factors for $|1\rangle^{\uparrow}_{M_U}$ and $|1\rangle^{\downarrow}_{M_D}$ are the same, i.e. $D^{\uparrow}_{M_U}(t) = D^{\downarrow}_{M_D}(t) = D_M(t)$. The SW entanglement state $\Psi^{\uparrow,\downarrow}_{M_{U,D}}(t)$ can be rewritten as,

$$\Psi^{\uparrow,\downarrow}_{M_{U,D}}(t) = D(t)\left(e^{-i\Delta\phi_S}\,|1\rangle^{\uparrow}_{M_U}|0\rangle + e^{-i\Delta\omega_0 t}e^{-i\delta\varphi(t)}\,|0\rangle\,|1\rangle^{\downarrow}_{M_D}\right)/\sqrt{2} \tag{16}$$

In our presented experiment, the phase difference $\delta\varphi_S$ is well passively stabilized. The frequency difference $\Delta\omega_0$ remains unchanged since the dc magnetic field B_0 is kept being constant. The phase difference fluctuation $\delta\varphi(t)$ will lead to decoherence of the entanglement state $\Psi^{\uparrow,\downarrow}_{M_{U,D}}(t)$, which will be shown by measuring the coherence between the retrieved fields as a function of storage time in the following.

By applying a read beam into the ensemble, the spin waves $|1\rangle^{\uparrow}_{M_U}$ and $|1\rangle^{\downarrow}_{M_D}$ will be converted into anti-Stokes fields a_{aS_U} and a_{aS_D}. As shown in Figure 3a, the retrieved field a_{aS_U} from the atoms is σ^--polarized, and it is changed into V–polarization after going through a wave plate $(\lambda/4)_{aS_U}$. While, the retrieved field aS_D from the atoms is σ^+-polarized, and it is changed into H–polarization after a wave plate $(\lambda/4)_{aS_D}$. The anti-Stokes field a_{aS_U} and a_{aS_D} are in a single-photon entangled state:

$$\Phi(t) \propto \left(e^{-i\Delta\phi_S - i\Delta\phi_{aS}}a^{\dagger}_{aS_U}|0\rangle|0\rangle + e^{-i\Delta\omega_0 t}e^{-i\delta\varphi(t)}a^{\dagger}_{aS_D}|0\rangle|0\rangle\right)/\sqrt{2} \tag{17}$$

where, $\Delta\phi_{aS}$ is the phase difference between a_{aS_U} and a_{aS_D} fields in propagation from the ensemble to BD_{aS}. which is passively stabilized in our presented experimental setup. The two anti-Stokes fields are combined into a spatial mode aS after BD_{aS}. Then, the mode aS goes through a wave plate $(\lambda/2)_{aS}$ and is directed into a polarization beam splitter PBS_{aS}. When measuring the coherence between the two spin waves, $(\lambda/2)_{aS}$ is set at 22.5^0. At this case, PBS_{aS} splits the input aS field into two modes $a_{aS1} = (a_{aS_U} + a_{aS_D})/\sqrt{2}$ and $a_{aS2} = (a_{aS_U} - a_{aS_D})/\sqrt{2}$, which are directed into the single-photon detectors D_{aS1} and D_{aS2}, respectively. After the retrieval, the atoms are prepared in $|g, m_F = 0\rangle$ again by the pumping pulses, and then the next trail starts. If no photon is detected by Ds_1, the pumping pulses are directly applied and the next trail starts.

4. Results

At first, we measure the cross-correlation function $g^{+,-}_{S,AS}$ ($g^{-,+}_{S,AS}$) between the $\sigma^+(\sigma^-)$ -polarized Stokes and σ^- (σ^+) -polarized anti-Stokes photons defined by $g^{+,-}_{S,aS} = P^{+,-}_{S,aS}/(P^{+}_{S}P^{-}_{aS})$ ($g^{-,+}_{S,aS} = P^{-,+}_{S,aS}/(P^{-}_{S}P^{+}_{aS})$), where $P^{+}_{S}(P^{-}_{S})$ and $P^{-}_{aS}(P^{+}_{aS})$ are the probabilities of detecting an σ^+ (σ^-) -polarized Stokes and σ^- (σ^+) -polarized anti-Stokes photon in U (D) arm, respectively, $P^{+,-}_{S,aS}$ ($P^{-,+}_{S,aS}$) is the coincidence probability between the σ^+ (σ^-) -polarized Stokes and σ^- (σ^+) -polarized anti-Stokes photons in U (D) arm. For measuring these quantities, $(\lambda/2)_S$ and $(\lambda/2)_{aS}$ are both set at 0^0, and the phase difference $\Delta\phi_S$ ($\Delta\phi_{aS}$) is compensated to be zero by using the phase compensator PC_S (PC_{aS}). The black squares in **Figure 4**a,b are the measured $g^{+,-}_{S,aS}$ ($g^{-,+}_{S,aS}$) data as a function of t. One can see that the measured $g^{+,-}_{S,aS}$ data are basically the same as the measured $g^{-,+}_{S,aS}$ data at various t and both decrease with t. Such decreases result from the SW decoherence caused by atomic motions. The red lines in Figures 4a and 5b are the fittings to the measured $g^{+,-}_{S,aS}$ and $g^{-,+}_{S,aS}$ according to (see Equation (S11) in Supporting information):

$$g^{+,-}_{S,aS} \approx 1 + \gamma^{\uparrow}(t)/\left(\chi\gamma^{\uparrow}(t) + \chi\left(1 - \gamma^{\uparrow}(t)\right)\xi_{se} + Z_{+}\right) \tag{18a}$$

$$g^{-,+}_{S,AS} \approx 1 + \gamma^{\downarrow}(t)/\left(\chi\gamma^{\downarrow}(t) + \chi\left(1 - \gamma^{\downarrow}(t)\right)\xi_{se} + Z_{-}\right) \tag{18b}$$

© 2023 The Authors. Advanced Quantum Technologies published by Wiley-VCH GmbH

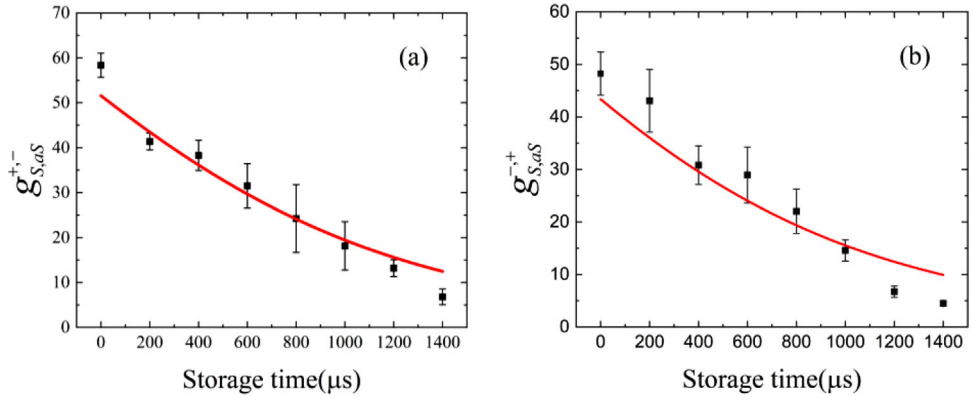

Figure 4. a,b) are the measured cross-correlation function $g^{+,-}_{S,AS}$ and $g^{-,+}_{S,AS}$ as a function of storage time t, respectively. The red lines are fittings based on Equations (18a) and (18b), where, $\zeta_- = 3.3 \times 10^{-4}$ and $\zeta_+ = 3.1 \times 10^{-4}$ are experimentally measured values. The fittings yield $\zeta_{se} = 0.26$.

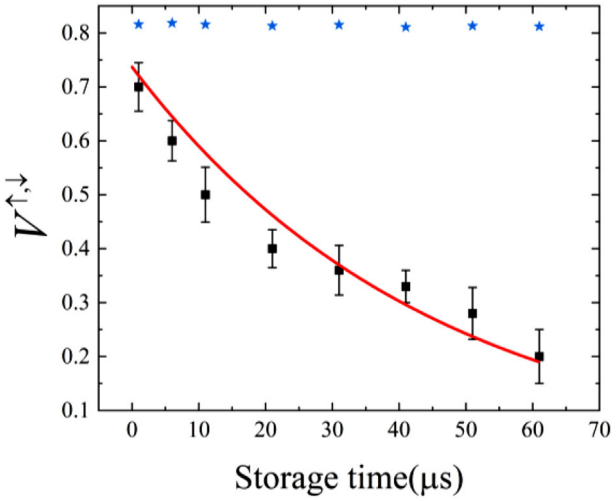

Figure 5. The measured visibility $V^{\uparrow,\downarrow}$ (black squares) as a fluctuation of storage time t. The red line is the fitting according to $V^{\uparrow,\downarrow} = V_g^{\uparrow,\downarrow}\xi' e^{-t/\tau_0}$. For comparison, we plot the calculated visibility data (blue stars) according to $V_g^{\uparrow,\downarrow} = \zeta(\bar{g}_{S,aS}(t) - 1)/(\bar{g}_{S,AS}(t) + 1)$, where, $\bar{g}_{S,aS}(t) = (g^{+,-}_{S,aS}(t) + g^{-,+}_{S,aS}(t))/2$ come from the measured data in Figure 4.

where, ξ_{se} denotes the branching ratio corresponding to the read-photon transitions, $Z_{\pm}$ the background noise in the $\sigma^{\pm}$-polarized anti-Stokes channels, $\gamma^{\uparrow}$ and $\gamma^{\downarrow}$ denote the retrieval efficiency of the MFI and MFS SWs, respectively. In the fittings, $\gamma^{\uparrow}$ and $\gamma^{\downarrow}$ values are taken from the measured data in Figure S1 in Supporting information.

To measure the visibility $V^{\uparrow,\downarrow}$ of the entanglement state $\Psi^{\uparrow,\downarrow}_{M_{U,D}}$, we set $(\lambda/2)_S$ and $(\lambda/2)_{aS}$ at 22.5^0. The counts of the retrieved photon at the detector D_{aS1} are recorded conditioned on a detection event at D_{S1}. When scanning the relative phase θ between the two anti-Stokes fields, the counts show an interference fringe and then we obtain the visibility. The black squares in **Figure 5** are the measured $V^{\uparrow,\downarrow}$ as a function of storage time t. The blue stars in Figure 5 are the calculated visibility according to $V_g^{\uparrow,\downarrow} = \zeta\frac{\bar{g}_{S,aS}(t)-1}{\bar{g}_{S,aS}(t)+1}$, where, $\bar{g}_{S,aS}(t) = (g^{+,-}_{S,aS}(t) + g^{-,+}_{S,aS}(t))/2$, ζ=0.85is the overlap between two arms. As shown in Figure 5, the measured $V^{\uparrow,\downarrow}$ rapidly decreases and while the calculated $V_g^{\uparrow,\downarrow}$ basically remains unchanged with the increase in the storage time t within the range from 5 to 60 μs. We explained this reason in the following. The calculated visibility according to $V_g^{\uparrow,\downarrow} = \zeta\frac{\bar{g}_{S,aS}(t)-1}{\bar{g}_{S,aS}(t)+1}$, which is given by the previous work,[25] doesn't include the decoherence process caused by SMFFs. While, the entangled state $\Psi^{\uparrow,\downarrow}_{M_{U,D}}(t)$, which is described in Equation (16), suffers from the decoherence process caused by SMFFs. Such decoherence process induces a faster decrease of visibility $V^{\uparrow,\downarrow}$ than that of the calculated $V_g^{\uparrow,\downarrow}$. Equation (13) gives the visibility of a single-excitation entanglement between two SWs including the decoherence caused by SMFFs. Based on the equation, we express the visibility $V^{\uparrow,\downarrow}$as $V^{\uparrow,\downarrow} = V_g^{\uparrow,\downarrow}e^{-t/\tau_0}$ where, $\tau_0 \sim (2\pi\mu_B\sigma_B/h)^{-1}$ is the lifetime limited by the slow magnetic-field fluctuation δB. The red solid line is the fitting to the measured $V^{\uparrow,\downarrow}$according to $V^{\uparrow,\downarrow} = V_g^{\uparrow,\downarrow}\xi' e^{-t/\tau_0}$, where ξ'=0.88 is a non-unit parameter, whose introduction is because that large difference of the Larmor frequency between the two spin waves causes a decrease in the coherence between two retrieval fields. The fittings yield lifetime $\tau_0 = 45\mu s$, which corresponds to rms width of $\sigma_B = 2.5mG$ according to $\tau_0 = (2\pi\mu_B\sigma_B/h)^{-1}$.

To demonstrate a scheme in which the phase difference noises between two SWs can be eliminated, we generate the second entanglement state that stores two SW modes in the MFS transitions. For which, we reset $(\lambda/4)_{S_U}$ in U arm, which makes the σ^--polarized S_U photon change into V-polarization. The V-polarized S_U field and the H-polarized S_D field combine into S mode after BD_S. Conditioned on a detection event at D_{S1}, the second entanglement state $\Psi^{\downarrow,\downarrow}_{M_{U,D}}(0) = \frac{1}{\sqrt{2}}(e^{-i\phi_s}|1\rangle^{\downarrow}_{M_U}|0\rangle + |0\rangle|1\rangle^{\downarrow}_{M_D}) + O(\chi)$ is created, where, $|1\rangle^{\downarrow}_{MU}$ ($|1\rangle^{\downarrow}_{MD}$) represents one SW excitation associated with the MFS coherence in $M_{U\ (D)}$ mode. After a storage time t, the heralded entanglement state $\Psi^{\downarrow,\downarrow}_{M_{U,D}}(0)$ is evolved into:

$$\Psi^{\downarrow,\downarrow}_{M_{U,D}}(t) = D(t)e^{-i\omega_0 t}e^{-i\delta\varphi(t)}\left(e^{-i\Delta\phi_s}|1\rangle^{\downarrow}_{M_U}|0\rangle + |0\rangle|1\rangle^{\downarrow}_{M_D}\right)/\sqrt{2} \quad (19)$$

© 2023 The Authors. Advanced Quantum Technologies published by Wiley-VCH GmbH

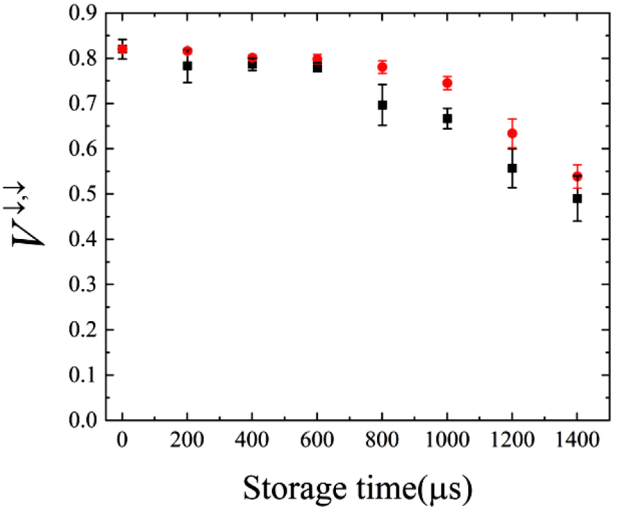

Figure 6. The measured visibilities $V^{\downarrow,\downarrow}$ (black squares) and the calculated visibilities (red circles) according to $V^{\downarrow,\downarrow} = \zeta(g^{-,+}_{S,AS}(t) - 1)/(g^{-,+}_{S,AS}(t) + 1)$ as a function of the storage time t.

where, ω_0 denotes the Larmor frequency caused by the bias magnetic field B_0 for either spin-wave modes alone with $\omega_0 = \omega_{U_0} = \omega_{D_0} == 2\pi\frac{\mu_B}{h}B_0$, the phase noise caused by SMFFs for mode M_U and M_D is the same i.e.,$\delta\varphi(t)_{M_U} = \delta\varphi(t)_{U_D} = \delta\varphi(t) = 2\pi\frac{\mu_B}{h}\delta Bt$ Thus, the visibility of the entanglement state $\Psi^{\downarrow,\downarrow}_{M_{U,D}}$ in Equation (19) is expressed as

$$V^{\downarrow,\downarrow} = \zeta\frac{g^{-,+}_{S,aS} - 1}{g^{-,+}_{S,aS} + 1} = V^{\downarrow,\downarrow}_{g} \tag{20}$$

which is not affected by SMFFs. Similar to the retrieval of the entangled state $\Psi^{\uparrow,\downarrow}_{M_{U,D}}(t)$, we apply the read beam to map the SWs $|1\rangle^{\downarrow}_{M_U}$ and $|1\rangle^{\downarrow}_{M_D}$ to the anti-Stokes photon in U and D arms, respectively. In the retrieval of $\Psi^{\downarrow,\downarrow}_{M_{U,D}}(t)$, the retrieved field in U arm is σ^+-polarized. So, we reset the wave plate $(\lambda/4)_{aS_D}$, which changes σ^--polarized anti-Stokes photon into V-polarization. The H-polarized anti-Stokes field in D arm and V-polarized anti-Stokes field in U arm are combined into a S mode by BD_{aS}. Similar to the measurement for $V^{\uparrow,\downarrow}$, we measure the visibility $V^{\downarrow,\downarrow}$ of the entanglement state $\Psi^{\downarrow,\downarrow}_{M_{U,D}}$. The black squares in **Figure 6** are the measured $V^{\downarrow,\downarrow}$as a function of storage time t. The red circles are the calculated visibilities according to $V^{\downarrow,\downarrow} = \zeta\frac{g^{-,+}_{S,AS}(t)-1}{g^{-,+}_{S,AS}(t)+1}$, where $\zeta = 0.84$. One can see that the measured data are well in agreement with the calculated data for various t, showing that the phase difference noise between the two SWs is eliminated. With the increase in the storage time t, the measured $V^{\downarrow,\downarrow}$ decreases, that is because $g^{-,+}_{S,AS}(t)$ decreases with t (see Figure 4b for details).

As pointed out in the above, the entanglement degree of the states $\Psi^{\uparrow,\downarrow}_{M_{U,D}}(t)$and $\Psi^{\uparrow,\downarrow}_{M_{U,D}}(t)$ are characterized by concurrence $C = \max(0, V(p_{01} + p_{10}) - 2\sqrt{p_{00}p_{11}}/P)$, where,$P = p_{01} + p_{10} + p_{00} + p_{11}$, p_{ij} corresponds to the probability to detect i anti-Stokes photons in U mode and j anti-Stokes photons in D mode. For the case $\chi << 1$, $p_{10} = p_{01} = p_c/2$, where, $p_c \approx \gamma(t)\eta$ is the conditional probability of detecting a photon in the anti-Stokes field from one spin-wave mode following a detection event for Stokes field, η is the efficiency for each detection channel.

The black squares in **Figure 7**a,b are the measured concurrences $C^{\uparrow,\downarrow}$ and $C^{\downarrow,\downarrow}$ for the states $\Psi^{\uparrow,\downarrow}_{M_{U,D}}(t)$ and $\Psi^{\downarrow,\downarrow}_{M_{U,D}}(t)$, respectively, as a function of the storage time t. The red and blue lines in Figure 7a,b are the calculated data according to ref. [25]

$$C^{\uparrow,\downarrow} \simeq \max\left[0, \bar{p}_c\left(V^{\uparrow,\downarrow} - 2\sqrt{(1-\bar{p}_c)/\bar{g}_{S,aS}}\right)\right] \tag{21a}$$

$$C^{\downarrow,\downarrow} \simeq \max\left[0, \bar{p}_c\left(V^{\downarrow,\downarrow} - 2\sqrt{(1-p_c)/g^{-,+}_{S,aS}}\right)\right] \tag{21b}$$

respectively, where, $\bar{p}_c = \eta(\gamma^{\uparrow} + \gamma^{\downarrow})/2$, $\bar{g}_{S,aS} = (g^{+,-}_{S,aS} + g^{-,+}_{S,aS})/2$, $\gamma^{\uparrow}$ ($\gamma^{\downarrow}$) denotes the retrieval efficiency from the MFI (MFS) SW. The fittings are in agreement with the measured data. The concurrences for both entanglement states degrade with t. One reason for this is the SW decoherence caused by the atomic random motions and magnetic-field gradient, which lead to decays of the cross-correlation functions $g_{S,aS}$ with t (Figure 4). The storage time for the concurrence $C^{\uparrow,\downarrow} \geq 0$ is ≈40 us, which is far less than that for the concurrence $C^{\downarrow,\downarrow} \geq 0$ (≈1.2 ms). We attributed this to that the entanglement state $\Psi^{\uparrow,\downarrow}_{M_{U,D}}(t)$ suffers from dephasing caused by SMFFs while the entanglement state $\Psi^{\downarrow,\downarrow}_{M_{U,D}}(t)$ does not.

5. Evaluating Decoherence Rate of Single-Excitation Entanglement Between Two Ensembles for Various Width of SMFFs

The protocol of the entanglement establishment between two ensembles has been shown in Figure 2. We assume that each repeater node (L or R ensemble) uses the state-of-art atomic SW memory system, where the atoms are loaded in an optical lattice and coupled into a cavity. In this case, the node memory has a single-mode initial efficiency of $\gamma_0 \approx 76\%$ and a lifetime of $\tau_D \approx 410$ms.[38] Its time-dependent retrieval efficiency can be approximately written as $\gamma(t) = \gamma_0 e^{-t/\tau_D}$. When obtaining such a long-lived SW memory, a bias magnetic field (≈4G) has to be applied onto the atoms to compensate the differential light shift.[38] The bias magnetic field can be produced by using Helmholtz coils driven with a DC power supply, which also generate SMFFs. In the individual ensembles, the rms width of SMFFs may be reduced to $\sigma_B \approx 2$mG by using low-noise supply, which is demonstrated in our presented experiment. It may also be reduced to $\sigma_B \approx 1$mG by using an active magnetic-field stabilization in ref.[72] and $\sigma_B \approx 0.2$mG via compensating the recorded magnetic-field noise with an open-loop feed-forward circuit in ref.[70]. In common cases, two current supplies are individually applied to R and L Helmholtz coils, respectively, and then SMFFs in R and L nodes are independent. So, the relative width of SMFFs between the two ensembles is $\sigma_\Delta = 2\sigma_B$. The sensitivity of the used clock coherence to the magnetic field in optical lattice atoms has been measured in ref.[71], which is $\mu' \approx 5$Hz/mG. Using the above parameters, we calculate the dependence of concurrence of entanglement for a repeater link on storage time t, which is shown in **Figure 8**. The green, blue, and red solid curves

© 2023 The Authors. Advanced Quantum Technologies published by Wiley-VCH GmbH

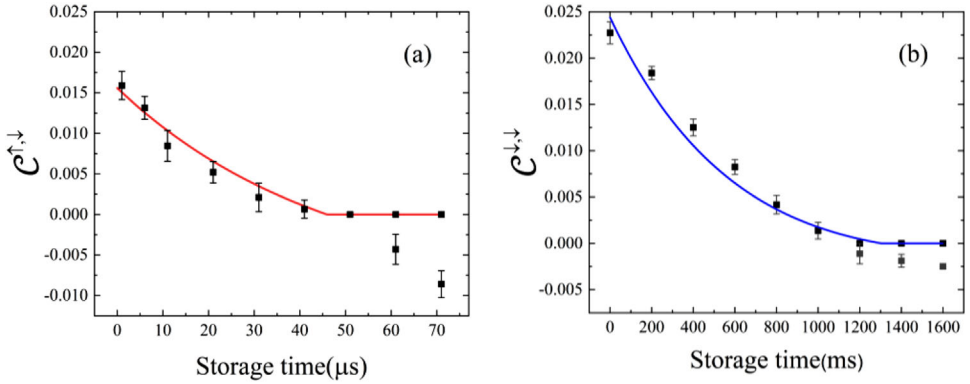

Figure 7. The black squares are the measured concurrences $C^{\uparrow,\downarrow}$ a) and $C^{\downarrow,\downarrow}$ b) as a function of storage time t. The red and blue lines are obtained from Equations (21a) and (21b), the retrieval efficiencies data come from Figure S1, Supporting Information.

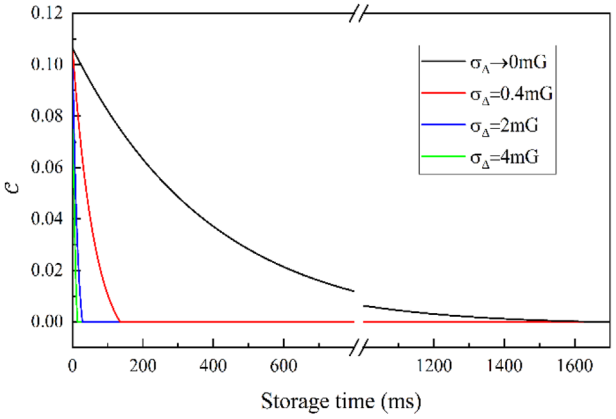

Figure 8. The calculated concurrence of single-excitation entanglement for a repeater link as a function of storage time t according to $C = \max[0, p_c(V - 2\sqrt{(1-p_c)/g_{S,aS}})]$, where, the visibility $V = \zeta(g_{S,aS}-1)/(g_{S,aS}+1)e^{-t/\tau_0}$, $\tau_0 = [2\pi\mu'(2\sigma_B)]^{-1} = (2\pi\mu'\sigma_\Delta)^{-1}$ is the lifetime limited by SFMMs in individual ensembles, $g_{S,aS} = 1 + \gamma(t)/(\chi\gamma(t) + \chi(1-\gamma(t))\xi_{se} + \zeta)$ is the cross-correlation function for either ensemble alone, $\zeta = 0.85$, the conditional probability $p_C = \gamma(t)\eta$, the retrieval efficiency is $\gamma(t) = \gamma_0 e^{-t/\tau_D}$ with $\gamma_0 = 76\%$ and $\tau_D = 410$ ms, the excitation probability and the background noise are assumed to be $\chi = 0.5\%$ and $\zeta = 3\times10^{-4}$per write pulse.

are the calculated $\mathscr{C}$ vs t for the magnetic-fluctuation differences with widths $\sigma_\Delta = 4$mG, $\sigma_\Delta = 2$mG, and $\sigma_\Delta = 0.4$mG. From these curves, we extract entanglement lifetimes (the storage time for $C > 0$) and show them in Table 1. As shown in Table 1, the lifetimes increase with the decrease in the widths, which shows the influence of SMFFs on the single-excitation entanglement. We propose a scheme to overcome such influence on the single-excitation entanglement storage in one link. Contrast to the common schemes, our scheme applies a single current supply to the Helmholtz coils at R and L nodes, which are connected in series. At each node, the slow magnetic-field fluctuation $\delta B(t)$ is proportional to the current fluctuations $\delta I(t)$ of the Helmholtz coils, i.e., $\delta B(t) \propto \delta I(t)$. We assume that the link has a typical length (separation distance between R and L nodes) of $d = 50$km. In this case, the frequency (with a range of 200-0Hz) of SMFFs is far less than $\frac{c}{d} \sim 6$kHz, which means that the current is quasi-steady, i.e., $\delta I_R(t) \approx \delta I_L(t)$. Also, we assumed that the scheme uses μ-metals to shield the residual field in R and L ensembles, respectively. In these cases, the difference between magnetic-field fluctuations in R and L nodes may be effectively eliminated, meaning that the width difference $\sigma_\Delta \to 0$. The black line in Figure 8 is the calculated concurrence of the single-excitation entanglement as storage time t for $\sigma_\Delta \to 0$, one can see that the lifetime of entanglement storage ($C > 0$) reaches to 1.7 s.

The quantum link efficiency η_{link} is defined as $\eta_{link} = T_S/T_G$, where T_G is the lifetime of entanglement storage for a link, T_S is the storage time of entanglement ($C > 0$). $\eta_{link} \geq 1$ promises a deterministic entanglement delivery,[17] which is critical for QR scaling. For a 50-km link, the required time for generating entanglement over the link via SPI is evaluated to be $T_G \approx 630ms$.[52] We calculate the lifetimes of single-excitation entanglement and the quantum link efficiencies for different σ_Δ and list them in **Table 1**. One can see that for the case of $\sigma_\Delta \to 0$, $\eta_{link} \approx 2.70$, which is greater than the threshold ($\eta_{link} \approx 1$) in ref. [17].

6. Discussion and Conclusion

We theoretically develop a SW model which includes not only the amplitude decoherence caused by atomic motions and inhomogeneous broadening of spin transition, but also phase noise induced by SMFFs. Based on the SW model, for a single-excitation entanglement between two atomic ensembles which forms a repeater link, we identify that the SMFF-induced phase noise will lead to entanglement decoherence. Such decoherence mechanism has not been pointed out in previous works on QRs.[2,22–24] With a cold atomic ensemble, we demonstrate a proof-in-principle experiment to verify our above view. In the experiment, we prepare single-excitation entanglement between two different SWs, named MFI and MFS SWs, and then demonstrate entanglement decoherence caused by SMFFs. Next, we demonstrate that single-excitation entanglement between two SWs stored in the same transition is immune from decoherence caused by SMFF, which shows the scheme can be used to suppress the SMFF-induced decoherence. In our presented experiment, the $1/e$ lifetime (≈800μs) of storing SWs is mainly limited to decoherence caused by atomic motions.

Based on our developed SW model, we next evaluate decoherence rate of single-excitation entanglement between two

© 2023 The Authors. Advanced Quantum Technologies published by Wiley-VCH GmbH

Table 1. The lifetimes of storing single-excitation entanglement T_S and quantum link efficiency η_{link} for various σ_Δ.

σ_B	2 mG	1 mG	0.2 mG	0 mG
$\sigma_\Delta = 2\sigma_B$	4 mG	2 mG	0.4 mG	0 mG
T_S	≈14 ms	≈28 ms	≈135 ms	≈1700 ms
$\eta_{link} = T_S/T_G$	≈0.02	≈0.04	≈0.21	≈2.70

remote ensembles suffering from individual SMFFs with the same rms widths. For suppressing decoherence of SW amplitude and achieving high retrieval efficiency, we assume that the atoms of each ensemble are loaded into an optical-lattice, and the magic field technique[71] as well as cavity-enhanced scheme are also applied to the ensembles.[27,38] Thus, each node has an initial retrieval efficiency of $\gamma_0 \approx 76\%$ and a $1/e$ lifetime of $\tau_D \approx 410$ms,[38] giving a time-depending efficiency of $\gamma(t) \approx \gamma_0 e^{-t/\tau_0}$.[38] For the case that the rms widths of slow magnetic-field fluctuations in individual ensembles are both $\sigma_B \approx 0.2$mG, the evaluated lifetimes of preserving entanglement ($\mathcal{C} > 0$) is 135 ms, where, the remained SMMFs is a main limitation.

We noted that the fluctuation width can be further reduced (for example, up to $\sigma_B = 0.1$mG) via synchronizing the experimental sequence with the mains electricity frequency 50 Hz in that experiment.[59,70] However, when using such noise-suppression technology in entanglement generation over a link, the experimental repeater rate has to be set at 50 Hz, which corresponds to a period of 20 ms. This period is far longer than the communication time (L / c) in a typical link, e.g., for a link with length L = 50 km, L/c = 0.25 ms. So, the use of such technology will greatly decrease the entanglement generation rate in the link. To eliminate SMFF-induced entanglement decoherence, we propose an approach, in which, the two Helmholtz coils used for the nodes in a link are connected in series and driven by a single DC supply. Such arrangements eliminate relative phase noise between two node memories. With the elimination of the relative phase noise, we evaluate lifetime of preserving entanglement ($\mathcal{C} > 0$) between the two memories, which is 1.7 s (see black curve in Figure 8).

An alternative effective method that protect the single-excitation entanglement from decoherence caused by SMFFs[12,17] is dynamical decoupling (DD) strategy. DD strategy realizes the protection by applying pulse sequence to repeatedly rotate two states of memory. Using this strategy, the storage lifetime of single-excitation entanglement between two remote single quantum systems (NV centers) has been significantly extended.[17] Recently, the storages of photonic time-bin qubits in a solid-state ensemble[69] and that of a weak laser pulse in cold atoms[17] used DD strategy to suppress inhomogeneous spin dephasing and then extend memory lifetime. The application of DD pulses to the ensembles will also suppress the SW phase noise caused by SMFFs. However, in atomic-ensemble-based memories, the DD application will lead to SW errors and introduce noise at memory output.[69] So, when using DD sequence including multiple pulses to suppress single-excitation entanglement decoherence in ensembles, the introduced noise will degrade the entanglement degree.

In summary, our work presents effective methods to suppress single-excitation entanglement decoherence induced by SMFFs in atomic-ensemble-based repeater link. We predict that the lifetime of preserving entanglement ($\mathcal{C} > 0$) between the two remote memories may reach 1.7 s, when the cavity-enhanced node memories in optical trap are employed, in which the two Helmholtz coils used for the nodes are connected in series and driven by a single DC supply. Our results would be of benefit in the optimal entanglement distribution policies in repeater chains.[74]

Supporting Information

Supporting Information is available from the Wiley Online Library or from the author.

Acknowledgements

This work was supported by the National Natural Science Foundation of China (12174235), the Fund for Shanxi Key Subjects Construction (1331), and the Fundamental Research Program of Shanxi Province (202203021221011)

Conflict of Interest

The authors declare no conflict of interest.

Data Availability Statement

All the data and calculations that support the findings of this study are available from the corresponding author upon reasonable request.

Keywords

atomic spin-wave, quantum repeater link, single-excitation entanglement, slow magnetic-field fluctuations

Received: May 25, 2023
Revised: July 10, 2023
Published online:

[1] L.-M. Duan, M. D. Lukin, J. I. Cirac, P. Zoller, *Nature* **2001**, *414*, 413.
[2] N. Sangouard, C. Simon, H. de Riedmatten, N. Gisin, *Rev. Mod. Phys.* **2011**, *83*, 33.
[3] C. Simon, *Nat. Photonics* **2017**, *11*, 678.
[4] H. J. Kimble, *Nature* **2008**, *453*, 1023.
[5] S. Wehner, D. Elkouss, R. Hanson, *Science* **2018**, *362*, 6412.
[6] S.-H. Wei, B. Jing, X.-Y. Zhang, J.-Y. Liao, C.-Z. Yuan, B.-Y Fan, C. Lyu, D.-L. Zhou, Y. Wang, G.-W. Deng, H.-Z. Song, D. Oblak, G.-C. Guo, Q. Zhou, *Laser Photonics Rev.* **2022**, *16*, 2100219.
[7] D. Gottesman, T. Jennewein, S. Croke, *Phys. Rev. Lett.* **2012**, *109*, 070503.

© 2023 The Authors. Advanced Quantum Technologies published by Wiley-VCH GmbH

[8] H.-J. Briegel, W. Dür, J. I. Cirac, P. Zoller, *Phys. Rev. Lett.* **1998**, *81*, 5932.
[9] F. Bussières, N. Sangouard, M. Afzelius, H. de Riedmatten, C. Simon, W. Tittel, *J. Mod. Opt.* **2013**, *60*, 1519
[10] A. I. Lvovsky, B. C. Sanders, W. Tittel, *Nat Photonics* **2009**, *3*, 706.
[11] W. Rosenfeld, F. Hocke, F. Henkel, M. Krug, J. Volz, M. Weber, H. Weinfurter, *Phys. Rev. Lett.* **2008**, *101*, 260403.
[12] M. Körber, O. Morin, S. Langenfeld, A. Neuzner, S. Ritter, G. Rempe, *Nat Photonics* **2018**, *12*, 18.
[13] B. B. Blinov, D. L. Moehring, L.-M. Duan, C. Monroe, *Nature* **2004**, *428*, 153.
[14] V. Krutyanskiy, M. Meraner, J. Schupp, V. Krcmarsky, H. Hainzer, B. Lanyon, *npj Quantum Inf.* **2019**, *5*, 72.
[15] D. L. Moehring, P. Maunz, S. Olmschenk, K. C. Younge, D. N. Matsukevich, L.-M. Duan, C. Monroe, *Nature* **2007**, *449*, 68.
[16] B. Hensen, H. Bernien, A. E. Dreau, A. Reiserer, N. Kalb, M. S. Blok, J. Ruitenberg, R. F. Vermeulen, R. N. Schouten, C. Abellan, W. Amaya, V. Pruneri, M. W. Mitchell, M. Markham, D. J. Twitchen, D. Elkouss, S. Wehner, T. H. Taminiau, R. Hanson, *Nature* **2015**, *526*, 682.
[17] P. C. Humphreys, N. Kalb, J. P. J. Morits, R. N. Schouten, R. F. L. Vermeulen, D. J. Twitchen, M. Markham, R. Hanson, *Nature* **2018**, *558*, 268.
[18] A. Delteil, Z. Sun, W.-B. Gao, E. Togan, S. Faelt, A. Imamoglu, *Nat. Phys.* **2016**, *12*, 218.
[19] K. Hammerer, A. S. Sørensen, E. S. Polzik, *Rev. Mod. Phys.* **2010**, *82*, 1041.
[20] A. Kuzmich, W. P. Bowen, A. D. Boozer, A. Boca, C. W. Chou, L.-M. Duan, H. J. Kimble, *Nature* **2003**, *423*, 731.
[21] J. Simon, H. Tanji, J. K. Thompson, V. Vuletic, *Phys. Rev. Lett.* **2007**, *98*, 183601.
[22] D. Felinto, C. W. Chou, H. de Riedmatten, S. V. Polyakov, H. J. Kimble, *Phys. Rev. A* **2005**, *72*, 053809.
[23] R. Zhao, Y. O. Dudin, S. D. Jenkins, C. J. Campbell, D. N. Matsukevich, T. A. B. Kennedy, A. Kuzmich, *Nat. Phys.* **2009**, *5*, 100.
[24] B. Zhao, Y.-A. Chen, X.-H. Bao, T, Strassel, C.-S. Chuu, X.-M. Jin, J. Schmiedmayer, Z.-S. Yuan, S. Chen, J.-W. Pan, *Nat. Phys.* **2009**, *5*, 95.
[25] J. Laurat, K. S. Choi, H. Deng, C. W. Chou, H. J. Kimble, *Phys. Rev. Lett.* **2007**, *99*, 180504.
[26] A. G. Radnaev, Y. O. Dudin, R. Zhao, H. H. Jen, S. D. Jenkins, A. Kuzmich, T. A. B. Kennedy, *Nat. Phys.* **2010**, *6*, 894.
[27] S.-J. Yang, X-J. Wang, X.-H. Bao, J.-W. Pan, *Nat. Photonics* **2016**, *10*, 381.
[28] E. Bimbard, R. Boddeda, N. Vitrant, A. Grankin, V. Parigi, J. Stanojevic, A. Ourjoumtsev, P. Grang, *Phys. Rev. Lett.* **2014**, *112*, 033601.
[29] M. Parniak, M. Dąbrowski, M. Mazelanik, A. Leszczyński, M. Lipka, W. Wasilewski, *Nat. Commun.* **2017**, *8*, 2140.
[30] H. Li, J. P. Dou, X. L. Pang, T. H. Yang, C. N. Zhang, Y. Chen, J. M. Li, X. M. Jin, *Optica* **2021**, *8*, 925.
[31] K. B. Dideriksen, R. Schmieg, M. Zugenmaier, E. S. Polzik, *Nat. Commun.* **2021**, *12*, 3699.
[32] C. Laplane, P. Jobez, J. Etesse, N. Gisin, M. Afzelius, *Phys. Rev. Lett.* **2017**, *118*, 210501.
[33] K. Kutluer, M. Mazzera, H. de Riedmatten, *Phys. Rev. Lett.* **2017**, *118*, 210502.
[34] D. N. Matsukevich, T. Chanelière, M. Bhattacharya, S.-Y. Lan, S. D. Jenkins, T. A. B. Kennedy, A. Kuzmich, *Phys. Rev. Lett.* **2005**, *95*, 040405.
[35] H. de. Riedmatten, J. Laurat, C. W. Chou, E. W. Schomburg, D. Felinto, H. J. Kimble, *Phys. Rev. Lett.* **2006**, *97*, 113603.
[36] Y. O. Dudin, A. G. Radnaev, R. Zhao, J. Z. Blumoff, T. A. B. Kennedy, A. Kuzmich, *Phys. Rev. Lett.* **2010**, *105*, 260502.
[37] S. Chen, Y.-A. Chen, B. Zhao, Z.-S. Yuan, J. Schmiedmayer, J.-W. Pan, *Phys. Rev. Lett.* **2007**, *99*, 180505.
[38] X.-J. Wang, S.-J. Yang, P.-F. Sun, B. Jing, J. Li, M.-T. Zhou, X.-H. Bao, J.-W. Pan, *Phys. Rev. Lett.* **2021**, *126*, 090501.
[39] S.-Z. Wang, M.-J. Wang, Y.-F. Wen, Z.-X. Xu, T.-F. Ma, S.-J. Li, H. Wang, *Commun. Phys.* **2021**, *4*, 168.
[40] Y-F Pu, N. Jiang, W. Chang, H-X Yang, C. Li, L-M Duan, *Nat. Commun.* **2017**, *8*, 15359.
[41] M.-J. Wang, S.-Z. Wang, T.-F. Ma, Y. Li, Y. Xie, H.-L. Jiao, H.-L. Liu, S.-J. Li, H. Wang, *Quantum* **2023**, *7*, 903.
[42] L. Tian, Z.-X. Xu, L.-R. Chen, W. Ge, H.-X. Yuan, Y.-F. Wen, S.-Z. Wang, S.-J. Li, H. Wang, *Phys. Rev. Lett.* **2017**, *119*, 130505.
[43] H. Zhang, X.-M. Jin, J. Yang, H.-N. Dai, S.-J. Yang, T.-M. Zhao, J. Rui, Y. He, X. Jiang, F. Yang, G.-S. Pan, Z.-S. Yuan, Y.-J. Deng, Z.-B. Chen, X.-H. Bao, S. Chen, B. Zhao, J.-W. Pan, *Nat. Photonics* **2011**, *5*, 628.
[44] E. Saglamyurek, N. Sinclair, J. Jin, J. A. Slater, D. Oblak, F. Bussières, M. George, R. Ricken, W. Sohler, W. Tittel, *Nature* **2011**, *469*, 512
[45] C. Clausen, I. Usmani, F. Bussières, N. Sangouard, M. Afzelius, H. de Riedmatten, N. Gisin, *Nature* **2011**, *469*, 508
[46] E. Saglamyurek, M. G. Puigibert, Q. Zhou, L. Giner, F. Marsili, V. B. Verma, S. W. Nam, L. Oesterling, D. Nippa, D. Oblak, W. Tittel, *Nat. Commun.* **2016**, *7*, 11202.
[47] K. T. Kaczmarek, P. M. Ledingham, B. Brecht, S. E. Thomas, G. S. Thekkadath, O. Lazo-Arjona, J. H. D. Munns, E. Poem, A. Feizpour, D. J. Saunders, J. Nunn, I. A. Walmsley, *Phys. Rev. A* **2018**, *97*, 042316.
[48] K. Heshami, D. G. England, P. C. Humphreys, P. J. Bustard, V. M. Acosta, J. Nunn, B. J. Sussman, *J. Mod. Opt.* **2016**, *63*, 2005.
[49] N. Sinclair, E. Saglamyurek, H. Mallahzadeh, J. A. Slater, M. George, R. Ricken, M. P. Hedges, D. Oblak, C. Simon, W. Sohler, W. Tittel, *Phys. Rev. Lett.* **2014**, *113*, 053603
[50] C. W. Chou, H. de Riedmatten, D. Felinto, S. V. Polyakov, S. J. van Enk, H. J. Kimble, *Nature* **2005**, *438*, 828.
[51] D. Lago-Rivera, S. Grandi, J. V. Rakonjac, A. Seri, H. de Riedmatten, *Nature* **2021**, *594*, 37
[52] Y. Yu, F. Ma, X.-Y. Luo, B. Jing, P.-F. Sun, R.-Z. Fang, C.-W. Yang, H. Liu, M.-Y. Zheng, X.-P. Xie, W.-J. Zhang, L.-X. You, Z. Wang, T.-Y. Chen, Q. Zhang, X.-H. Bao, J-W Pan, *Nature* **2020**, *578*, 240.
[53] Z.-S. Yuan, Y.-A. Chen, B. Zhao, S. Chen, J. Schmiedmayer, J.-W. Pan, *Nature* **2008**, *454*, 1098
[54] X. Liu, J. Hu, Z.-F Li, X. Li, P.-Y. Li, P.-J. Liang, Z.-Q. Zhou, C.-F. Li, G.-C. Guo, *Nature* **2021**, *594*, 41.
[55] B. Zhao, Z.-B. Chen, Y.-A. Chen, J. Schmiedmayer, J.-W. Pan, *Phys. Rev. Lett.* **2007**, *98*, 240502.
[56] C.-W. Chou, J. Laurat, H. Deng, K. S. Choi, H. de Riedmatten, D. Felinto, H. J. Kimble, *Science* **2007**, *316*, 1316.
[57] B. Julsgaard, A. Kozhekin, E. S. Polzik, *Nature* **2001**, *413*, 400.
[58] D.-S. Ding, W. Zhang, Z.-Y. Zhou, S. Shi, B.-S. Shi, G.-C. Guo, *Nat. Photonics* **2015**, *9*, 332.
[59] X.-Y. Luo, Y. Yu, J.-L. Liu, M.-Y. Zheng, C.-Y. Wang, B. Wang, J. Li, X. Jiang, X.-P. Xie, Q. Zhang, X.-H. Bao, J.-W. Pan, *Phys. Rev. Lett.* **2022**, *129*, 050503.
[60] S. Ritter, C. Nölleke, C. Hahn, A. Reiserer, A. Neuzner, M. Uphoff, M. Mücke, E. Figueroa, J. Bochmann, G. Rempe, *Nature* **2012**, *484*, 195
[61] T. Leent, M. Bock, F. Fertig, R. Garthoff, S. Eppelt, Y. Zhou, P. Malik, M. Seubert, T. Bauer, W. Rosenfeld, W. Zhang, C. Becher, H. Weinfurter, *Nature* **2022**, *607*, 69.
[62] P. Xu, H.-L. Yong, L.-K. Chen, C. Liu, T. Xiang, X.-C. Yao, H. Lu, Z.-D. Li, N.-L. Liu, L. Li, T. Yang, C.-Z. Peng, B. Zhao, Y.-A. Chen, J.-W. Pan, *Phys. Rev. Lett.* **2017**, *119*, 170502.
[63] Y.-F. Pu, S. Zhang, Y.-K. Wu, N. Jiang, W. Chang, C. Li, L.-M. Duan, *Nat. Photonics* **2021**, *15*, 374.
[64] Y.-W. Cho, G. T. Campbell, J. L. Everett, J. Bernu, D. B. Higginbottom, M. T. Cao, J. Geng, N. P. Robins, P. K. Lam, B. C. Buchler, *Optica* **2016**, *3*, 100

© 2023 The Authors. Advanced Quantum Technologies published by Wiley-VCH GmbH

[65] G. Heinze, C. Hubrich, T. Halfmann, *Phys. Rev. Lett.* **2013**, *111*, 033601
[66] J. J. Longdell, E. Fraval, M. J. Sellars, N. B. Manson, *Phys. Rev. Lett.* **2005**, *95*, 063601
[67] A. Holzäpfel, J. Etesse, K. T. Kaczmarek, A. Tiranov, N. Gisin, M. Afzelius, *New J. Phys.* **2020**, *22*, 063009
[68] Y. Ma, Y.-Z. Ma, Z.-Q. Zhou, C.-F. Li, G.-C Guo, *Nat. Commun.* **2021**, *12*, 2381
[69] A. Ortu, A. Holzäpfel, J. Etesse, M. Afzelius, *npj Quantum Inf.* **2022**, *8*, 29
[70] S. Ried, M. Lettner, C. Vo, S. Baur, G. Rempe, S. Dürr, *Phys. Rev. A* **2012**, *85*, 022318.
[71] Y. O. Dudin, R. Zhao, T. A. B. Kennedy, A. Kuzmich, *Phys. Rev. A* **2010**, *81*, 041805(R)
[72] W. Rosenfeld, J. Volz, M. Weber, H. Weinfurter, *Phys. Rev. A* **2011**, *84*, 022343.
[73] C.-W. Chou, Degree Thesis, California Institute of Technology **2006**.
[74] Á. G. Iñesta, G. Vardoyan, L. Scavuzzo, S. Wehner, *npj Quantum Inf.* **2023**, *9*, 46.

© 2023 The Authors. Advanced Quantum Technologies published by Wiley-VCH GmbH